J Appl Electrochem (2010) 40:691–699
DOI 10.1007/s10800-009-0044-7

ORIGINAL PAPER

Electrochemical and physical characterisation of lead-based anodes in comparison to Ti–(70%) IrO_2/(30%) Ta_2O_5 dimensionally stable anodes for use in copper electrowinning

Z. S. Msindo · V. Sibanda · J. H. Potgieter

Received: 12 May 2009 / Accepted: 23 November 2009 / Published online: 9 December 2009

Abstract The suitability of various dimensionally stable anodes (DSAs®) was investigated in comparison to the conventional lead alloy anodes in the electrowinning of copper. DSA® plate and mesh specimens of composition Ti–(70%) IrO_2/(30%) Ta_2O_5 and lead–(6%) antimony were evaluated. The electrochemical behaviour of these anodes was studied by carrying out open circuit potential measurements, galvanostatic chronopotentiometry, cyclic voltammetry and chronoamperometry. Physical characterisation was done using a scanning electron microscope. It was observed that the DSA® plate anode exhibited the highest corrosion resistance followed by the DSA® mesh and lead anodes, respectively. The results also showed that during copper electrowinning using lead anodes, dissolution of the anode occurs while for both DSAs® marginal loss of coating was observed. The lead anode had the highest anode potential followed by the DSA® plate and mesh anodes, respectively. Overall, it was demonstrated that the DSA® plate anode is the most suitable anode for copper electrowinning.

Keywords Electrowinning · Dimensionally stable anodes · Oxygen overvoltage · Electrochemical behaviour · Lead anodes

Z. S. Msindo · V. Sibanda (✉)
Department of Chemical and Metallurgical Engineering, University of the Witwatersrand, Private Bag 3, Wits 2050, South Africa
e-mail: vusumuzi.sibanda@wits.ac.za

J. H. Potgieter
School of Biology, Chemistry and Health Sciences, Manchester Metropolitan University, Manchester M15 6BH, UK

1 Introduction

The essential requirements for anodes in electrowinning are electrochemical stability in sulphate electrolytes, resistance to the chemical effects of oxygen liberated on the anode surface, low oxygen overvoltage, mechanical stability and structural integrity under operating conditions, product quality and environmental safety [1, 2]. The traditional anodes of choice in the electrowinning industry have been lead-based anodes with typical compositions such as lead–antimony (6%), lead–calcium (0.7%)–tin (1.3%) and lead–strontium (0.05%)–tin (0.6%). The continued use of the lead-based anodes in the electrowinning process has been mainly due to their relatively low cost compared to other materials. However, certain drawbacks in the use of these anodes have been documented, while some of their undesirable physical and chemical characteristics have prompted further research into alternative materials to replace them.

The main disadvantages of lead-based anodes are their high energy consumption and low corrosion resistance. Corrosion results in shorter anode life spans and production of poor quality cathode deposits due to the incorporation of lead corrosion products [3]. Considering the low cost of lead-based anodes, it is important that any replacement anodes offer high energy savings and low corrosion rates. Various measures have been proposed by researchers to reduce energy consumption and cathode contamination during copper electrowinning. These include replacement of the conventional anode reaction with an oxidation reaction of SO_2 [4], or Fe^{2+} ions [5, 6], addition of Co^{2+} ions to the electrolyte in the conventional cell [7] and the use of alternative anodes [3, 8–11].

The anodic oxidation of sulphite ions which are formed by the dissolution of sulphur dioxide in the aqueous

electrolyte results in a reduction of 1.06 V versus the Standard Hydrogen Electrode (SHE) from the reversible half-cell potential for oxygen evolution (1.23 V versus SHE) [4], as shown in the equations below:

$$H_2SO_3 + H_2O \rightarrow SO_4^{2-} + 4H^+ + 2e^- \quad E^0 = 0.17\,V \text{ versus SHE} \tag{1}$$

$$H_2O \rightarrow 2H^+ + 1/2O_2 + 2e^- \quad E^0 = 1.23\,V \text{ versus SHE} \tag{2}$$

However, despite the significant reduction in reversible potential, Pace and Stauter [4] found that at high current densities, the slow kinetics of the oxidation reaction of SO_2 results in a high anode overvoltage which is less advantageous than that indicated by thermodynamic considerations. The anodic oxidation of Fe^{2+} ions, as an alternative anode reaction, has also been found to produce poor quality cathode copper, and furthermore, also causes a loss in current efficiency due to the reduction of Fe^{3+} to Fe^{2+} at the cathode and re-oxidation of Fe^{2+} to Fe^{3+} [12, 13]. The generation of acid used in the leaching process would also be affected [14]. Loutfy and Leroy [15] mentioned that the most promising measures of these are reduction of the reversible potential by careful selection of the overall cell reaction, and overvoltage reduction through the use of activated anodes (DSAs®).

Dimensionally stable anodes (DSAs®) consist of mixed metal oxide coatings, usually on titanium or nickel substrates. The oxides that can be used in the oxide coatings include tantalum oxide (Ta_2O_5), iridium oxide (IrO_2), ruthenium dioxide (RuO_2), and tin oxide (SnO_2) [16–19].

To date, many researchers have studied the characteristics of DSA® electrodes in great detail in search of the most suitable DSA®-type electrode for oxygen evolution in acidic solutions. Comninellis and Vercesi [16] examined the microstructural properties, electrocatalytic activity and anodic stability of nine binary coatings with IrO_2, RuO_2 and Pt as conducting components, and TiO_2, ZrO_2, Ta_2O_5 as inert oxides on titanium as the substrate. The techniques used included X-ray diffractometry, cyclic voltammetry and accelerated life tests, respectively. These authors concluded that the Ti/IrO_2 (70 mol%)–Ta_2O_5 (30 mol%) coating was the best electrode for oxygen evolution in acidic media since it was associated with high catalytic activity and service life. The service life of Ti/IrO_2–Ta_2O_5 with 70 mol% IrO_2 was estimated to be 5–10 years [20]. Several authors have also found that the IrO_2–Ta_2O_5 coated titanium electrode with a 70% Ir/30% Ta mole ratio composition was one of the best electrode materials evaluated to date in processes involving oxygen evolution [8, 21, 22]. Work has also been reported on the corrosion behaviour of lead-based anodes in base metal electrolytes, although no comparisons were made with other anode materials such as the Ti/IrO_2 (70 mol%)–Ta_2O_5 (30 mol%) anodes [23, 24].

Studies comparing DSA® anodes of different compositions to the lead-based anodes have also been carried out in base metal electrolytes by some researchers. In one study done by Cooper [25], potentiodynamic polarisation experiments carried out in an electrolyte containing 50 g L^{-1} Cu and 50 g L^{-1} H_2SO_4 showed that a reduction of 500–600 mV versus SHE in overvoltage could be realised with dimensionally stable anodes (DSAs®) compared to the conventional lead–antimony anodes. However, in this case, the actual composition of the DSAs® used in the experiments was not revealed. Loutfy and Leroy [15] carried out polarisation experiments using the TiO_2/RuO_2 DSA® and an antimonial lead anode in 200 g L^{-1} sulphuric acid and found that the anode potential for the lead alloy anode was 500 mV (versus SHE) higher than that of the TiO_2/RuO_2 anode. Kulandaisamy et al. [26] also carried out potentiodynamic studies in 2 M sulphuric acid and achieved about 450 mV reduction versus Hg/Hg_2SO_4/0.5 M H_2SO_4 in anode potential using the Ti/Ir–Co anode compared to the lead anode. Ramachandran et al. [27] investigated the Ti/IrO_2 anode and the lead–silver (1%) anode in zinc electrowinning. These authors observed that the Ti/IrO_2 DSA® anode exhibited a reduction in anode potential of 500 m V versus SHE over the lead anode, thus leading to an energy saving of about 15%. Pavlović and Dekanski [28] also investigated the performance of lead-based anodes against Ti/Pt–IrO_2, Ti/RuO_2, Ti/Pt–IrO_2–MnO_2, Ti/Pt–IrO_2–PbO_2, Ti/Pt–IrO_2–RuO_2, Ti/MnO_2, Ti/RuO_2–MnO_2 and Ti–PbO_2 dimensionally stable anodes in zinc electrowinning and hard chromium plating baths. They observed that the titanium anode coated with Pt, IrO_2 and/or RuO_2 showed the best properties of low energy consumption and high current efficiency.

However, despite these previous investigations, no data comparing the Ti/IrO_2 (70 mol%)–Ta_2O_5 (30 mol%) anodes and lead anodes in copper electrowinning has been documented. Furthermore, different research papers are produced using data and anode materials acquired under different experimental procedures and operating parameters (electrolyte composition, temperature, etc.). DSAs® with the same chemical composition may show different behaviour, since electrochemical performance was found to be influenced strongly by the preparation procedure and parameters, such as pre-treatment of the substrate [22, 29, 30], precursor solution [31], coating application method [22] and sintering treatment [32–35].

Therefore, in the present article comparisons are made between the lead–antimony (6%) anode and Ti–(70%) IrO_2/(30%) Ta_2O_5 plate and mesh specimens based on anode surface characteristics, corrosion rates, anode

potential, anode stability, electrocatalytic activity and morphology in synthetic copper electrowinning (55 g L^{-1} Cu and 100 g L^{-1} H_2SO_4). These anodes were tested in order to provide information on the most suitable anode for industrial processing of copper electrolyte at an Anglo Platinum operation. Open circuit potential (OCP) measurements, galvanostatic chronopotentiometry, chronoamperometry and cyclic voltammetry were the electrochemical techniques employed during these experiments. This research also focused on the Ti–(70%) IrO_2/(30%) Ta_2O_5 DSA® mesh anode which showed the ability to significantly reduce energy consumption in copper electrowinning when compared to the Ti–(70%) IrO_2/(30%) Ta_2O_5 DSA® plate and lead–antimony (6%) anodes.

2 Experimental

2.1 Electrochemical characterisation

Open circuit potential, galvanostatic chronopotentiometry tests, chronoamperometry and cyclic voltammetric (CV) techniques were used to study the electrochemical properties and surface characteristics of the anodes. These tests were conducted at room temperature (rt). The electrochemical cell used in the study was a 500 mL Pyrex beaker, covered with a perspex lid with three openings through which the working electrode (WE), counter electrode (CE) and reference electrode (RE) could be inserted. The CE was a graphite rod. A silver/silver chloride electrode (0.222 V vs. standard hydrogen electrode, SHE) was used as the RE. The electrochemical tests were performed with an Autolab, potentiostat/galvanostat (Eco Chemie)/PGSTAT302 controlled by General Purpose Electrochemical System 4.9 (GPES) software, installed on a personal computer. The test electrolytes used in the study were 0.5 M sulphuric acid solution and a synthetic solution containing 55 g L^{-1} copper in 100 g L^{-1} sulphuric acid. All solutions were freshly prepared using distilled water and analytical reagent grade copper sulphate and sulphuric acid. In the galvanostatic tests, copper deposits were obtained at the required conditions for a period of 2 h using a stainless steel plate of dimensions 12 cm × 2 cm × 1 cm as cathode.

2.2 Physical characterisation

The surface morphology of the DSAs® and antimonial lead anodes were analysed using a JSM-840 (JEOL) scanning electron microscope. Morphological studies were carried out in order to establish the relationship between surface morphology and anode behaviour.

3 Results and discussions

3.1 Open circuit potential measurements

In the OCP tests, a two electrode arrangement, involving the WE (anode specimen) and RE was used. This was accomplished by physically disconnecting the CE, since the net current in OCP tests should be zero. The potential resulting from the electrochemical reactions occurring at the anode-solution interface, was then recorded by the potentiostat for a period of 2 h for each anode specimen. OCP measurements were carried out in order to assess the stability of the anodes under investigation. The tests also provided information on the anode material with the highest corrosion resistance and the redox transitions controlling the surface electrochemistry of the anodes. Figure 1 shows the curves for OCP measurements for the DSA® anodes and lead anode.

The results show that for the DSA® plate, there was a small but sharp decrease initially in the potential from 0.49 to 0.45 V within the first 200 s, after which the potential stabilised for the remaining duration of the measurement. The initial decrease in OCP can be attributed to the erosion of coating particles that are weakly bonded to the substrate once there is interaction between the electrolyte and the anode [8]. For the DSA® mesh, the potential shifted rapidly towards the more noble potentials from 0.33 to 0.41 V within the first 3750 s and then stabilised. For the antimonial lead specimen, there was a small increase of the potential from 0.08 to 0.10 V for the whole duration of the experiment.

The DSA® anodes had nobler potentials compared to the lead alloy anode, with the DSA® plate having the largest average OCP value of 0.44 V. From these results, it can be concluded that the DSA® plate has the highest corrosion resistance followed by the DSA® mesh and lastly the lead alloy anode.

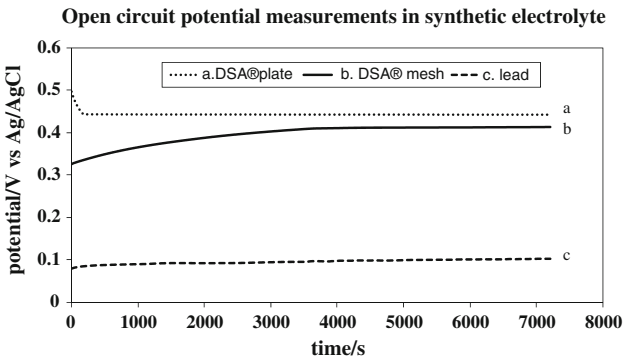

Fig. 1 OCP curves for Ti–IrO_2/Ta_2O_5 plate, Ti–IrO_2/Ta_2O_5 mesh and Pb/Sb in 55 g L^{-1} Cu and 100 g L^{-1} H_2SO_4 at room temperature (rt)

OCP measurements also provided information about the electrodes' surface active sites. Comparison of the OCP values with the theoretical value of the standard potential for the solid-state transitions present in the coating suggested that the surface electrochemistry for the DSA® anodes could be controlled by a hydrated Ir(III)/Ir(IV) redox transition as shown in Eq. 3.

$$2\ IrO_2 + 2H^+ + 2e^- \Leftrightarrow Ir_2O_3 + H_2O \quad E^0 = +0.6\ \text{V versus SHE} \tag{3}$$

Similar results have been observed by Wen and Hu [36], Alves et al. [37] and Chen and Trasatti [38] for DSA® electrodes with IrO_2 as catalyst.

For the lead anodes, the surface electrochemistry was found to be controlled by the Pb/Pb(II) redox transition shown in Eq. 4.

$$Pb + SO_4^{2-} \rightarrow PbSO_4 + 2e^- + H^+ \quad E^0 = +0.356\ \text{V versus SHE} \tag{4}$$

A micrograph of a used lead–antimony anode, taken by a scanning electron microscope in this study also substantiates this result. This is shown in Fig. 2.

Moskalyk et al. [39] also mentioned that with lead anodes, lead sulphate is formed on the wetted surface of the anodes during electrowinning. This $PbSO_4$ layer can reach half a centimetre in thickness and eventually flakes off, leading to contamination of the cathode deposit. Similar observations have also been made on the lead anode in a lead acid battery by other researchers [40].

3.2 Galvanostatic chronopotentiometry

In galvanostatic chronopotentiometry, a constant current was applied between the auxiliary and WE. The WE potential was recorded with time with respect to the RE. Figure 3 compares the performance of the DSA® anodes (Ti–Ta_2O_5/IrO_2) and the traditional Pb–Sb (6%) under oxygen evolution conditions. The lead anode was found to be associated with the highest anode potential of 1.97 V. This may be due to its higher oxygen overpotential. When the anode potentials for the DSA® plate and mesh anodes were compared with that of the lead anode they were found to be 19 and 24% lower, respectively. The differences observed in the anode potentials of the three anodes may be attributed to the nature of these anodes, since in the experiments the electrolyte composition, electrode distance, temperature, cathode material and current density were kept constant. As previously mentioned, studies involving comparisons of the lead-based anodes and DSAs® of various compositions have shown that significant energy savings can be achieved with the DSAs® [15, 25–28]. However, there has been no previous direct comparison between the Ti–Ta_2O_5/IrO_2 plate and mesh anodes with the lead–antimony anode.

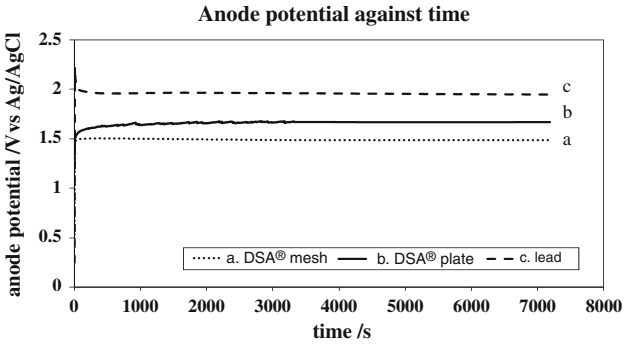

Fig. 3 Anode potential–time curves for Pb–Sb (6%) and Ti–Ta_2O_5/IrO_2 (plate and mesh) in 55 g L^{-1} Cu and 100 g L^{-1} H_2SO_4 at 190 A m^{-2}

3.2.1 *Electrolyte contamination*

Electrode stability was also evaluated under these galvanostatic conditions. Electrolyte contamination is a direct measure of how much an anode deteriorates or corrodes during electrowinning. The respective electrolytes for the

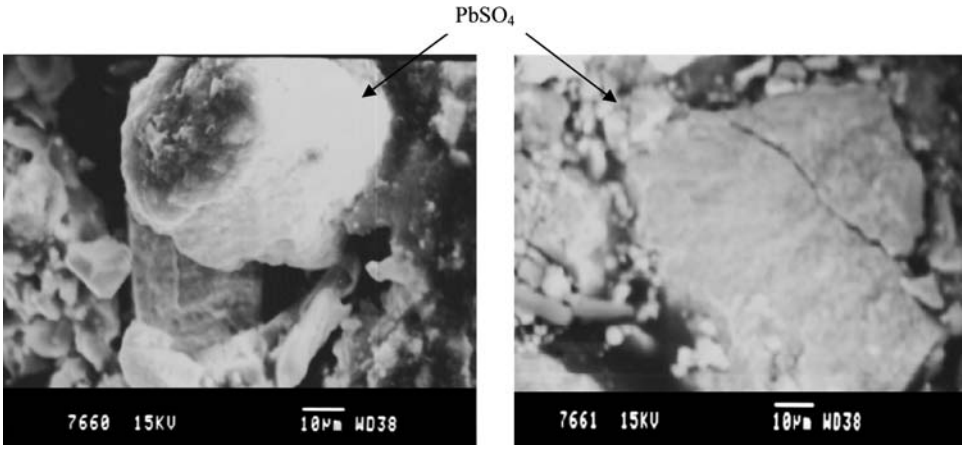

Fig. 2 SEM micrographs for a used lead–antimony anode

Table 1 Concentrations of lead, titanium, tantalum and iridium in the electrolytes containing the lead–antimony anode, DSA® plate and mesh anodes

Anode type	Element	Average concentration (ppm)	Standard deviation
Lead–antimony	Pb	6.867	0.1
DSA® plate	Ti	0.017	0.001
	Ta	0.001	0.0002
	Ir	0.003	0.0002
DSA® mesh	Ti	0.015	0.001
	Ta	0.000	nd
	Ir	0.004	0.0002

nd Not determined

experiments done with the three anodes were analysed for lead (Pb–Sb anode) and titanium, iridium and tantalum contamination (for DSA® anodes) after 2 h of galvanostatic tests, by using an Atomic Absorption Spectrometer (AAS). The results are shown in Table 1.

The results in Table 1 indicated that anodic dissolution of lead occurs during the electrowinning of copper with lead alloy anodes. The lead ions in solution are most likely to result in cathode contamination when they form lead sulphate, which in turn attaches to the growing copper deposit. Anodic dissolution may also contribute to a reduced life span for the anodes, and varying current distribution due to changing electrode thickness and flatness. The resultant lead sludge that must be removed from the cells, and handled with severe environmental constraints, is also a major problem. Ramachandran et al. [27] reported that the corrosion of the lead anodes is mainly responsible for the lead content of a zinc deposit in the electrowinning of zinc. Moskalyk et al. [39] also reported similar observations.

The presence of traces of tantalum (coating stabiliser) and iridium (active component) reported in Table 1, also shows that, during electrowinning operations using DSA® anodes, some marginal loss of coating occurs. The amount of iridium loss was three times greater than the tantalum loss, probably due to the high stability of tantalum in the coating. Traces of the titanium substrate were also detected in the samples analysed. The amount of iridium loss in the electrochemical cell containing the DSA® mesh anode was slightly greater than the iridium loss in the cell containing the DSA® plate specimen. This can possibly be attributed to the larger electrochemically active surface area (EASA) of mesh anodes. A greater EASA, results in more area being available for corrosion. Hu et al. [41] investigated the degradation mechanism of Ti–(70%) IrO_2/(30%) Ta_2O_5 anodes in H_2SO_4 and found that the deactivation mechanism of these anodes during electrolysis occurred in three stages, namely; active, stable and de-active. In the first two stages, the dissolution of the coating dominated (with IrO_2 component preferentially lost compared to Ta_2O_5).

3.3 Cyclic voltammetry

Cyclic voltammetry (CV) was used to investigate the surface characteristics and EASA of the anodes. The voltammetric charge, obtained by integration between the hydrogen and the oxygen gas evolution region of a CV curve, has been shown to be proportional to the EASA of metal oxide electrodes, and also gives a measure of the number of active sites [7, 41, 42]. All experiments were carried out in 0.5 M sulphuric acid at a scan rate of 20 mV s^{-1}. These results can be correlated to usual processes in the copper electrolyte [43].

3.3.1 Cyclic voltammograms for lead anodes

For the lead anode, curves were generated over a potential range of −0.5 to 2.2 V versus Ag/AgCl, which covers reactions from metallic lead Pb^0 to Pb(IV) and oxygen evolution. This is graphically illustrated in Fig. 4. All curves showed two anodic peaks during scanning in a positive direction and two cathodic peaks when scanning in the negative direction. The first process which takes place is the anodic dissolution of lead and the formation of a $PbSO_4$ layer, which has passivating properties. This is followed by a wide passive region. As the anodic potential increases to about 1.75 V, lead (IV) oxide forms at the surface of the electrode. With a further increase in the potential, O_2 evolution commences around 1.9 V.

Oxygen evolution was found to intensify with an increase in the number of cycles. The cathodic peak which appeared at 1.4 V in the reverse scan could be attributed to the reduction of PbO_2 (which formed on the surface) back to $PbSO_4$. Another small cathodic peak at −0.5 V could be the result of the reduction of $PbSO_4$ to Pb. These results are synonymous to what other authors have reported [44, 45].

3.3.2 Cyclic voltammograms for DSA® anodes

Figure 5 shows the CV curves for DSA® mesh and plate anodes in 0.5 M H_2SO_4 solution at a scan rate of 20 mV s^{-1}. The curves were recorded between −0.6 to 1.5 V versus Ag/AgCl which covers the reactions of hydrogen evolution, Ir(III)/Ir(IV) and oxygen evolution.

It can be seen that the CV curves all have a similar shape. Several current peaks were present in both voltammograms. The anodic peak at a potential of ≈1.5 V is due to the oxygen evolution reaction, while the cathodic peak at a potential of about −0.6 V is indicative of

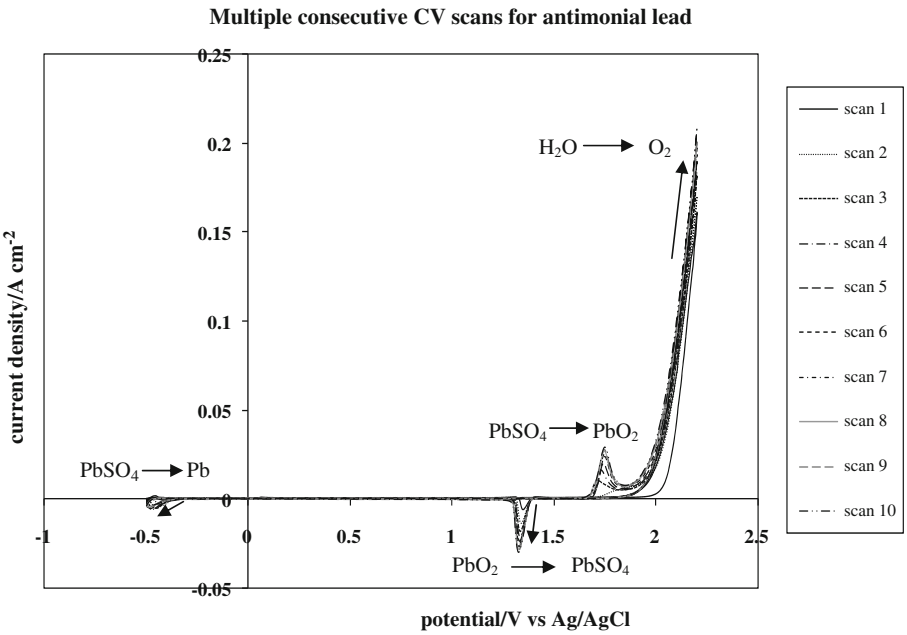

Fig. 4 Cyclic voltammograms for the lead alloy anode

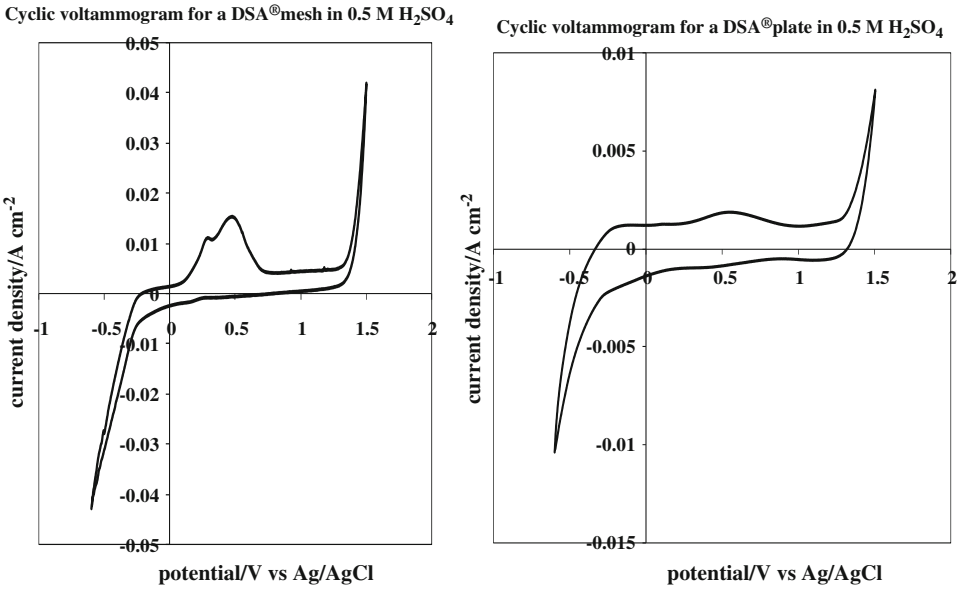

Fig. 5 Cyclic voltammograms for Ti/IrO_2–Ta_2O_5 electrodes

intensive hydrogen evolution. A pair of peaks observed at potentials between 0.3 and 0.5 V for the DSA® mesh anode is likely to be a result of the redox transition Ir(III)/Ir(IV), while for the DSA® plate anode a smaller current peak appearing around 0.5 V is also attributed to the same redox transition, which occurs to a lesser extent. Xu and Scantlebury [46] also observed intense hydrogen evolution and Ir(III)/Ir(IV) redox transition peaks on the Ti/IrO_2 (70 mol%)–Ta_2O_5 (30 mol%) anode in 1 M H_2SO_4 solution in the potential range −0.6 to 1.2 V and at a scan rate of 20 mV s^{-1}. The results are in agreement with those of Mattos-Costa et al. [47] and Oliveira-Sousa et al. [48].

3.3.3 *Electrochemically active surface area*

Table 2 shows the voltammetric charges, q^*, measured at a scan rate of 20 mV s^{-1} for the three anode specimens in the potential range of 0–1.5 V versus Ag/AgCl. The mesh anode had the greatest q^* value, followed by the DSA® plate anode and the lead anode, respectively. The results indicate that the mesh has the largest working area for oxygen evolution followed by the DSA® plate anode and the lead anode, respectively.

The working area of an anode is dependent on the structure of the anode itself. Dimensionally stable anodes

Table 2 Voltammetric charges for the anode specimens

Anode specimen	q^*(mC cm^{-2})
Ti/IrO_2–Ta_2O_5 plate	51
Ti/IrO_2–Ta_2O_5 mesh	226
Pb/Sb	26

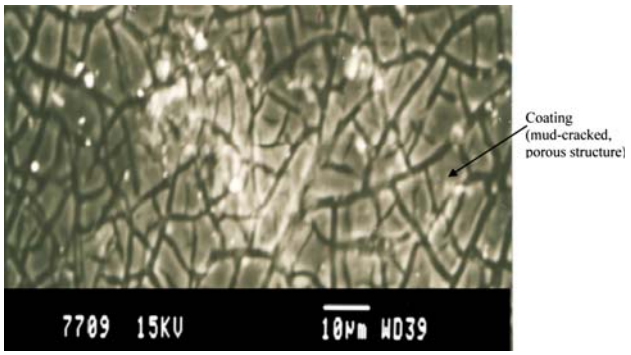

Fig. 6 SEM micrograph for dimensionally stable anodes

have a mud cracked, porous structure which enhances their working area (EASA) compared to lead alloy anodes which have an almost homogenous surface, as shown in Figs. 6 and 7, respectively. A larger working area results in increased catalytic activity in electrode processes. The high activity facilitates a lowering of the effective current density, resulting in a reduced anode potential [26]. This explains why the anode potentials for the DSA® plate and mesh anodes were 19 and 24% lower, respectively, when compared with that of the lead anode (Fig. 3).

Xu et al. [34], found values of 40.56 and 50.03 mC cm^{-2} for q^* using the Ti/IrO_2 (70 mol%)–Ta_2O_5 (30 mol%) plate anodes in 1 M H_2SO_4 solution at a scan rate of 20 mV s^{-1}. However, there has been no documented data on typical values of q^* for the Ti/IrO_2 (70 mol%)–Ta_2O_5 (30 mol%) mesh and lead anodes.

3.3.4 *Determination of double layer capacitance*

The double layer capacitance was determined by evaluating the slopes of the graphs of current density against scan rate at a potential of 1.0 V versus Ag/AgCl, where no main redox transitions occurred on the surface [46]. Figure 8 indicates that a linear relationship exists between current density and scan rate for the DSA® anodes. This was also seen in Xu and Scantlebury's work [46]. Similarly to the anodic charge, q^*, the DSA® mesh had a higher double layer capacitance than the rest. Therefore, C_{dl} can also be used to describe the EASA of both the DSA® anodes [46]. The value of the double layer capacitance for the Ti/IrO_2

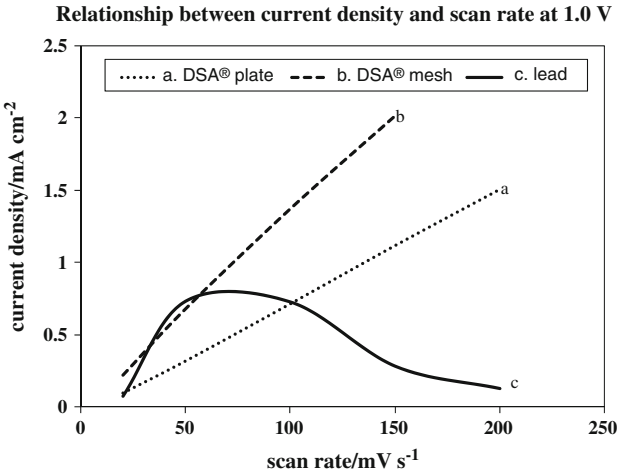

Fig. 8 Relationship between current density and scan rate at a fixed potential of 1.0 V versus Ag/AgCl for Ti/IrO_2–Ta_2O_5 and Pb/Sb anodes

Fig. 7 SEM micrographs for a lead alloy anode

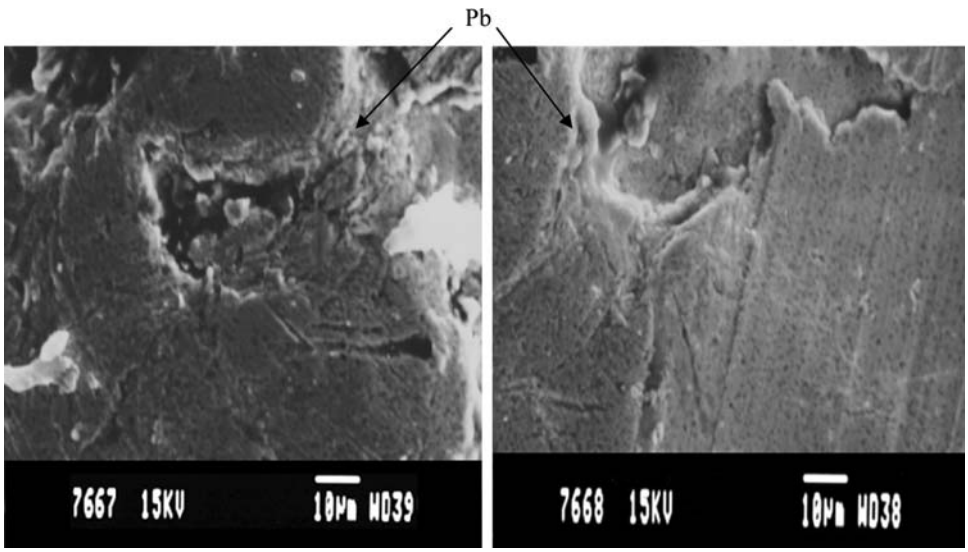

Table 3 Double layer capacitance and roughness factor for DSAs®

Electrode	C_{dl} (mF cm^{-2})	Roughness factor (RF)
Ti/IrO_2–Ta_2O_5 plate	8.0	133
Ti/IrO_2–Ta_2O_5 mesh	12.8	213

(70 mol%)–Ta_2O_5 (30 mol%) plate determined in this work was different from the value found by Xu and Scantlebury [46], who reported a value of 23.6 mF cm^{-2} in sodium sulphate solution. This could be the result of the methods of preparation of these anodes. No data on double layer capacitance for the Ti/IrO_2 (70 mol%)–Ta_2O_5 (30 mol%) mesh anode has been documented previously.

For the lead anode specimen, the relationship between current density and scan rate showed a large deviation from linearity. Therefore, its double layer capacitance, C_{dl}, could not be evaluated. No work has been previously reported on the relationship between current density and scan rate for lead-based anodes.

The roughness factor for the DSA® anodes was calculated by dividing the values of the double layer capacitance by 60 μF cm^{-2}, which is the value for a smooth and compact TiO_2 film with a rutile structure [49]. Table 3 shows the capacitances and roughness factors for the DSAs®. The RF value for the Ti/IrO_2–Ta_2O_5 mesh was 60% greater than that of the Ti/IrO_2–Ta_2O_5 plate. This suggested that the structure of oxide anodes has an effect on surface roughness and consequently the EASA. RF values in the range 83–395 have also been reported by other researchers in the field [46].

3.4 Chronoamperometry (<1 s)

Chronoamperometry (1 s) was used for the rapid characterisation of the three anodes in synthetic electrolyte, as shown in Fig. 9. The results showed that upon applying a potential step of 1.5 V versus Ag/AgCl, the resulting oxygen evolution reaction (OER) currents initially decreased and quickly reached a quasi steady-state value. For the DSA® anodes, the decrease in current density represented the dissolution of the active component occurring during electrolysis. As penetration of the electrolyte occurred through the mud cracked, porous structure of the thermally prepared oxide layer, the DSA® anodes became stable around 0.3 s. From these results, it can be concluded that the electrocatalytic activity of DSA® anodes decreases slowly with time as a consequence of coating dissolution, until deactivation is reached by base metal passivation. For the lead alloy anode, the initial decrease in current density was likely a result of the partial blockage of the electrode surface due to the formation of a passivating layer. As the layer grew in thickness, the anode stabilised, as evidenced by the constant current density at 0.05 s. No data on chronoamperometry tests for the three anode materials investigated in this study is available from other sources in the field.

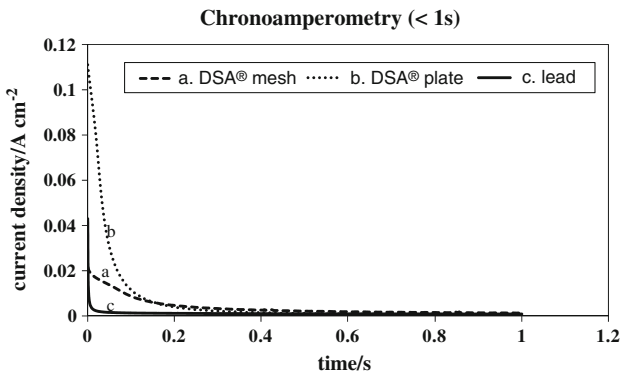

Fig. 9 Chronoamperometry tests in synthetic electrolyte

4 Conclusions

Electrochemical tests were carried out on DSA® and lead anodes in order to determine the most suitable anode based on stability and energy consumption in the electrowinning of copper. The following key findings were made:

- The DSA® plate anode has the highest corrosion resistance followed by the DSA® mesh anode and lastly the lead alloy anode.
- The surface electrochemistry for both DSA® anodes is controlled by the Ir(III)/Ir(IV) redox transition while the surface electrochemistry for the lead anodes is controlled by the Pb/Pb(II) redox transition.
- Since anode potential is a major component of the cell voltage, it implies that if lead anodes are replaced by DSA® anodes (plate and mesh) which have low anode potentials, energy savings of around 19–24% could be realised.
- Significant lead anode dissolution occurs during the electrowinning of copper.
- The failure mechanism of DSA® anodes not only involves passivation but also coating consumption.
- The DSA® mesh anode has the largest working area for oxygen evolution, followed by the DSA® plate and lead anodes, respectively.

Based on these findings, the DSA® plate anode would be the most suitable anode in the electrowinning of copper, in comparison to the conventional lead-based anode and the DSA® mesh anode, because not only does it exhibit a reasonably low energy consumption, but also a high corrosion resistance.

Acknowledgements The authors would like to acknowledge the financial support provided by Anglo Research and the School of

Chemical and Metallurgical Engineering at the University of the Witwatersrand.

References

1. Gupta CK, Mukherjee TK (1990) Hydrometallurgy in extraction processes, vol 2. CRC Press, Florida
2. Weems D, Schledorn M, Farmer MD (2005) Electrodes Int Inc Tech Rep
3. Moats M, Hardee K, Brown C (2003) J Miner Metal Mater Soc 55:46–48
4. Pace GF, Stauter JC (1974) Can Min Metall Bull 67:85–91
5. Liddell DM (1926) Handbook of nonferrous metallurgy, vol 2. McGraw-Hill, New York
6. Cooke AV, Chilton JP, Fray DJ (1981) Extraction Metall 81: 430–441
7. Panda B, Das SC, Panda RK (2009) J Hydrometall 95:87–91
8. Rolewicz J, Comninellis Ch, Plattner E, Hinden J (1988) J Electrochim Acta 33:573–580
9. Hrussanova A, Mirkova L, Dobrev Ts (2001) J Hydrometall 60:199–213
10. Ferdman A (2000) US Patent 6129822
11. Tuffrey N, Fletcher H, Marinovich Y, McGinnity J (2006) AMIRA Proj
12. Das SC, Gopala KP (1996) Int J Miner Process 46:91–105
13. Biswas AK, Davenport WG, King M, Schlesinger M (2002) Extractive metallurgy of copper, 4th edn. Pergamon, Oxford
14. Moats M, Free M (2007) J Miner Metal Mater Soc 59:34–36
15. Loutfy RO, Leroy RL (1978) J Appl Electrochem 8:549–555
16. Ch Comninellis, Vercesi GP (1991) J Appl Electrochem 21:335–345
17. Morimitsu M, Tamura H, Matsunaga M, Otogawa R (2000) J Appl Electrochem 30:511
18. Yang CH, Lee CC, Wen TC (2000) J Appl Electrochem 30:1043
19. Rubel M, Haasch R, Mrozek P et al (1994) Vacuum 45:423
20. Mráz R, Krýsa J (1994) J Appl Electrochem 24:1262–1266
21. Hu JM, Zhang JQ, Cao CN (2003) Thermochim Acta 403:257
22. Otogawa R, Morimitsu M, Matsunaga M (1998) Electrochim Acta 44:1509
23. Cifuentes G, Cifuentes L, Crisostomo G (1998) Corr Sci 40: 225–234
24. Saber TMH, Shams el din AM (1968) Electrochim Acta 13: 937–945
25. Cooper WC (1985) J Appl Electrochem 15:789–805
26. Kulandaisamy S, Prabhakar RS, Chockalingam SC et al (1997) J Appl Electrochem 27:579–583
27. Ramachandran P, Nandakumar V, Sathaiyan N (2004) J Chem Tech Biotechnol 79:578–583
28. Pavlović MG, Dekanski A (1997) J Solid State Electrochem 1:208–214
29. Mahe E, Devilliers D (2000) Electrochim Acta 46:629
30. Chu LY, Xu LK, Wu LB et al (2005) Acta Metall Sin 41:763
31. Terezo AJ, Pereira EC (2002) Mater Lett 53:339
32. Foti G, Mousty C, Reid V, Comninellis Ch (1998) Electrochim Acta 44:813
33. Kristóf J, Szilágyi T, Horváth E et al (2004) Thermochim Acta 413:93
34. Xu L, Xin Y, Wang J (2009) Electrochim Acta 54:1820–1825
35. Martelli GN, Ornelas R, Faita G (1994) Electrochim Acta 39:1551–1558
36. Wen TC, Hu CC (1992) J Electrochem Soc 139:2158
37. Alves VA, da Silva LA, Boodts JFC (1998) Electrochim Acta 44:1525
38. Chen H, Trasatti S (1993) J Appl Electrochem 23:559
39. Moskalyk RR, Alfantazi A, Tombalakian AS, Valic D (1999) Miner Eng 12:65–73
40. Chung DDL (2003) Composite materials: science and applications. Springer, London
41. Hu CC, Lee CH, Wen TC (1996) J Appl Electrochem 26:72–82
42. Zanta CLPS, de Andrade AR, Boodts JFC (2000) J Appl Electrochem 30:667
43. Yu P, O'Keefe JO (1999) J Electrochem Soc 146:1361–1369
44. Yamamoto Y, Fumino K, Ueda T, Namu M (1992) Electrochim Acta 37:199
45. Czerwi A, Elazowska M, Grde M et al (2000) J Power Sources 85:49–55
46. Xu LK, Scantlebury JD (2003) J Electrochem Soc 150:B288–B293
47. Mattos-Costa FI, de Lima-Neto P, Machado SAS, Avaca LA (1998) Electrochim Acta 44:1515
48. de Oliveira-Sousa A, da Silva MAS, Machado SAS et al (2000) Electrochim Acta 45:4467
49. Bulhoes LO, Abeid LM, Boodts JF (1997) J Electrochem Soc 144:3348–3354